Excitation of P-Modes in the Sun and Stars

Robert Stein, Dali Georgobiani and Regner Trampedach
Michigan State University

Hans-Günter Ludwig
Lund Observatory

Åke Nordlund
Astronomical Observatory, NBIfAFG

July 17, 2003

Abstract. P-mode oscillations in the Sun and stars are excited stochasticly by Reynolds stress and entropy fluctuations produced by convection in their outer envelopes. The excitation increases with increasing effective temperature (until envelope convection ceases in the F stars) and also increases with decreasing gravity.

Keywords: Oscillations, P-Modes, Excitation, Sun, Stars

1. Introduction

Acoustic (p-mode) oscillations have been observed in the Sun and several other stars (Deubner 1975, Bedding & Kjeldsen 2003). They are excited by entropy (non-adiabatic gas pressure) fluctuations and Reynolds stress (turbulent pressure) fluctuations produced by convection in the stellar envelopes. Expressions for the excitation rate have been derived by several people (Goldreich & Keeley 1977; Balmforth 1992; Goldreich, Murray & Kumar 1994; Nordlund & Stein 2001; Samadi & Goupil 2001). Evaluation of these expressions depends on knowing the properties of the convection. To obtain analytic results it is necessary to make drastic approximations to the convection properties. Unfortunately, both mixing length theory (Bohm-Vitense 1958) and more recent theories of Canuto (Canuto & Mazzitelli 1991) do not adequately describe the dynamics of convection and in addition contain free parameters and so lack predictive capability. Using results of numerical simulations of the near surface layers of a star it is possible to calculate the excitation rate of p-modes for the Sun and other stars without the need to make such approximations.

Here we describe the expression for the stochastic excitation of p-mode oscillations derived by Nordlund & Stein (2001) (sec. 2) and the simulations used to derive the stellar convective properties (sec. 3). We briefly present the properties of stellar envelope convection relevant to the excitation of oscillations (sec. 4). Next the formula for

p-mode excitation is applied to the Sun (sec. 5). The results are in good agreement with observations. Excitation decreases at low frequencies because of increasing mode mass and decreasing mode compressibility. Excitation decreases at high frequencies because convection lacks high frequency motions. Finally, we apply our formula to the excitation of stellar p-mode oscillations using simulations of nine stars near the main sequence and a cool sub-giant (sec. 6). We find that the total excitation over the entire star increases with increasing effective temperature and decreasing surface gravity.

2. Excitation Rate

The excitation rate can be derived by evaluating the PdV work of the non-adiabatic gas and turbulent pressure (entropy and Reynolds stress) fluctuations on the modes (Nordlund & Stein 2001). This is a stochastic process, so the pressure fluctuations occur with random phases with respect to the oscillation modes. Therefore the excitation expression must be averaged over all possible relative phases. The resulting rate per unit area is (Nordlund & Stein 2001)

$$\frac{\Delta\langle E_\omega\rangle}{\Delta t} = \frac{\omega^2 \left|\int_r dr \delta P^*_\omega \frac{\partial \xi_\omega}{\partial z}\right|^2}{8\Delta\nu E_\omega} \ . \tag{1}$$

Here δP^*_ω is a Fourier component of the non-adiabatic, incoherent pressure fluctuations. The pressure is the sum of turbulent pressure (Reynolds stress) and non-adiabatic gas pressure (entropy) fluctuations,

$$\delta P = \delta P_{\rm turb} + \delta P^{\rm nad}_{\rm gas} \ , \tag{2}$$

where the turbulent pressure fluctuation is

$$\delta P_{\rm turb} = \delta\langle \rho \delta V_{\rm z}^2\rangle \ , \tag{3}$$

and the non-adiabatic gas pressure fluctuation is

$$\delta P^{\rm nad}_{\rm gas} = P_{\rm gas}\left(\delta \ln P_{\rm gas} - \Gamma_1 \delta \ln \rho\right) \ . \tag{4}$$

The turbulent and non-adiabatic gas pressure fluctuations are calculated from the simulation at each 3D location at each saved time. The velocity, density and internal energy are obtained directly from the saved simulation data and the Γ_1 is found from the equation of state table. They are then averaged over horizontal planes and interpolated to the Lagrangian frame comoving with the mean radial motion at each time. The fluctuations δP are the variations from their time average.

ξ_ω is the mode displacement eigenfunction and $\omega\partial\xi/\partial z$ is the mode compression. The mode energy is

$$E_\omega = \frac{1}{2}\omega^2 \int_r dr\ \rho\ \xi_\omega^2 \left(\frac{r}{R}\right)^2 \ . \tag{5}$$

The mode eigenfunctions are evaluated from a complete envelope model, obtained by fitting the mean simulation radial structure to a deeper one-dimensional, adiabatic, convective envelope model. $\Delta\nu = 1/(\text{total time interval})$ is the frequency resolution with which δP_ω is computed.

Our expression for the mode excitation rate is similar to the one derived by Goldreich, Murray & Kumar (1994)

$$\frac{dE_\omega}{dt} = \omega^2 \int d^3r \left|\frac{d\xi}{dr}\right| \int_0^{h_{\max}} h^2 dh \tau_h \left[\left(\rho v_{\rm h}^2\right)^2 + \left(\left(\frac{\partial P}{\partial s}\right)_\rho \delta s_{\rm h}\right)^2\right] \ , \tag{6}$$

where the eigenfunctions are already normalized, as well as to the one derived by Samadi and Goupil (2001)

$$\frac{dE}{dt} = \frac{1}{8M} \int d^3x \nabla^i \xi^j \nabla^\ell \xi^m \int d\tau e^{-i\omega\tau} \int d^3r \left[\langle\ \rho^2 u_i' u_j' u_\ell'' u_m'' \rangle + \delta_{ij}\delta_{\ell m} \langle q' q'' \rangle\right] \ , \tag{7}$$

where

$$q = \left(\frac{\partial P}{\partial s}\right) \nabla \cdot (s_t \mathbf{u}) \ ,$$

and the mode mass is

$$M = \int d^3\rho\, |\xi|^2 \ .$$

3. The Simulations

We simulate a small portion of the photosphere and the upper layers of the convection zone by solving the equations of mass, momentum and energy conservation. Spatial derivatives are calculated using third order splines vertically and 5th order compact derivatives horizontally on a non-staggered grid. Time advance is a third order leapfrog scheme (Hyman 1979; Nordlund & Stein 1990). The calculation is stabilized by explicit diffusion in all the conservation equations using a hyperviscosity which enhances the diffusion on the scale of a few grid zones and decreases it for larger scale variations.

A significant, sometimes dominant, form of energy near the top of surface convection zones in stars is ionization energy. Hence, we use a tabular equation of state which includes LTE ionization and excitation

of hydrogen and other abundant elements and the formation and ionization of H_2 molecules. This is necessary to obtain the correct relation between energy flux and fluid velocities and temperature fluctuations.

Radiative energy exchange is critical in determining the structure of the upper convection zone. Escaping radiation cools the plasma that reaches the surface, which produces the low entropy plasma whose buoyancy work drives the convection. Since the top of the convection zone occurs near the level where the continuum optical depth is one, neither the optically thin nor the diffusion approximations give reasonable results. We need to solve the 3D, LTE, non-gray radiation transfer in our models (Nordlund 1982, Stein & Nordlund 2003). To obtain the radiative heating and cooling, the Feautrier equations are integrated along one vertical and 4 slanted rays (which are rotated each time step) through each grid point on the surface with the opacity and Planck functions interpolated to the intersection of the rays with each horizontal plane. The radiative transfer calculation is sped up by drastically reducing the number of wavelengths at which we solve the Feautrier equations, by using a multi-group method where the opacity at different wavelengths is collected into 4 bins according to its magnitude, with the Planck (source) function similarly binned. As a result, all wavelengths in a given bin have optical depth unity at approximately the same geometrical depth so that integrals over optical depth commute with the sum over wavelengths.

The boundaries of the computational domain are "virtual boundaries". The region we simulate is, in reality, coupled to an external medium, about which we have no information, and is influenced by what happens there. Given our lack of information on what is occurring outside our computational domain, the best that can be achieved are boundary conditions that are stable and introduce few artifacts. Horizontal boundaries are periodic – what goes out one side comes in the other. This allows the formation of granules and mesogranules, but removes the effect of supergranular flows on our calculation. Vertical boundaries are transmitting, with the entropy of the inflowing fluid at the bottom of the domain specified (which fixes the energy flux). Since ascending plasma below the superadiabatic layer is nearly isentropic and uniform and since convection is driven from the thin thermal boundary layer where energy transport switches between convective and radiative at the top of the convection zone which is included in our domain, the unknown influences from the external regions are small.

Simulations have been made of the Sun, 6 solar like stars (Trampedach et al. 1998), an F V, K V and K IV stars (Ludwig & Nordlund 2000), all with solar composition. Since the simulation domains are shallow, only a few eigenmodes are present. To obtain all the eigenfunctions

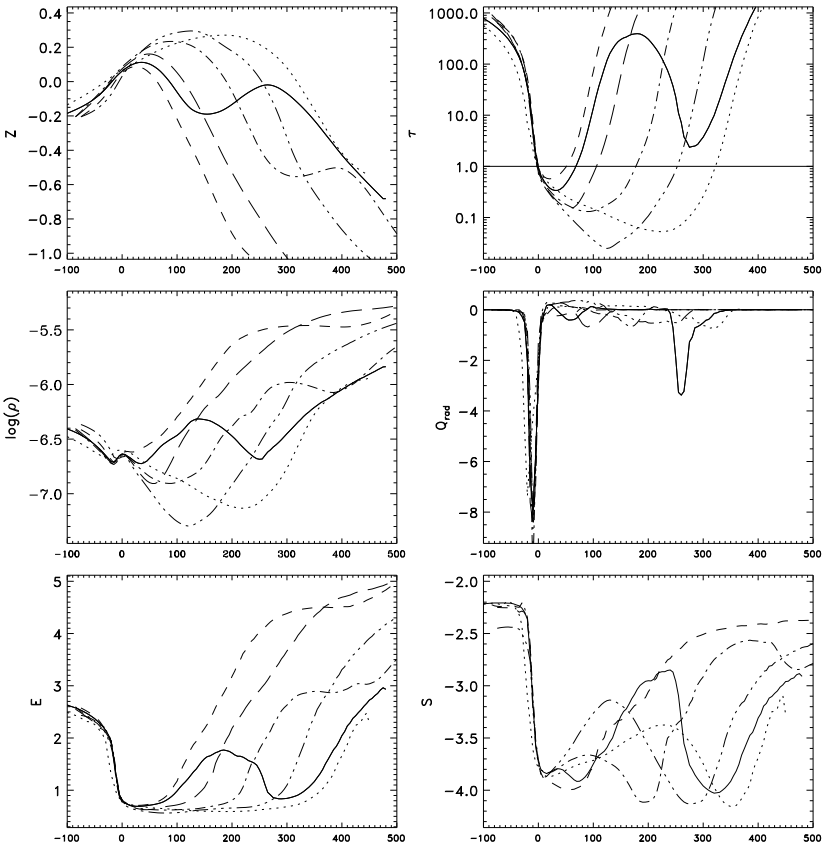

Figure 1. History as a function of time (s) of 6 fluid parcels that reach the solar surface: height (Mm), optical depth, $\log(\rho)$, radiative heating (10^3 ergs/gm/s), internal energy (10^5 ergs/gm), and specific entropy (10^8 ergs/gm/K). When fluid reaches optical depth $\tau \sim 100$, it begins to cool rapidly. It recombines. Its entropy and energy drop and its density increases. As it heads down into the interior it heats up by adiabatic compression, by diffusive energy exchange and by entraining overturning, high entropy, ascending fluid.

the deeper portions of the stellar envelopes must be included. For the solar-like stars the envelopes were extended inwards by matching the mean structure from the 3D simulations to 1D mixing length envelope models. The eigenfunctions of the other three stars were calculated from pure 1D mixing length models which match the entropy jump in the hydrodynamical simulations.

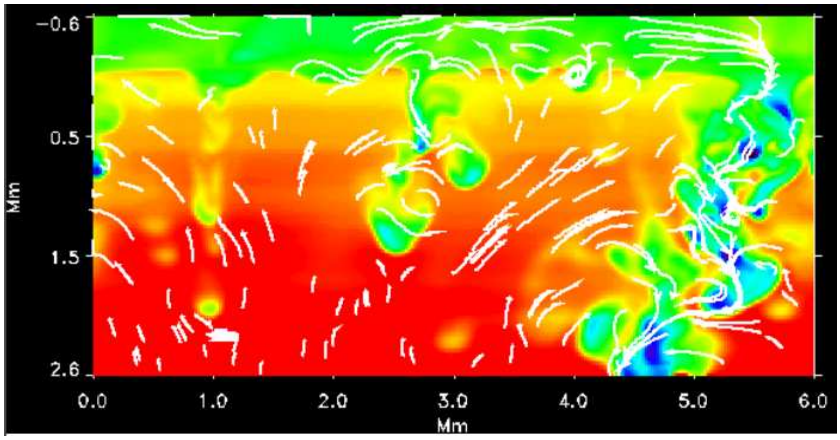

Figure 2. Temperature fluctuations and flow velocities on a vertical slice through the simulation domain. Red is hot and blue is cool. The fairly laminar upflows and turbulent downflows are clear.

4. Convection Properties

Convection is driven by radiative cooling in the thin thermal boundary layer near the stellar surface. Only the fluid that reaches within a few photon mean free paths of the surface radiates away its energy and entropy (Fig. 1). This low entropy fluid that has lost its energy near the surface is denser than its surroundings and is pulled back down into the interior by gravity. It forms the cores of downdrafts. These cool, low entropy, filamentary, turbulent, downdrafts plunge many scale heights through warm, entropy neutral, smooth, diverging, fairly laminar upflows (Fig. 2). (See Stein & Nordlund 1998, 2000 for more details.) The downdrafts, which are turbulent and have the largest entropy variations (Figs. 3 – 5), are the site of most of the excitation of the p-mode oscillations (Stein & Nordlund 2001).

5. Excitation of Solar Oscillations

To obtain the total excitation rate for the entire Sun we multiply the excitation rate per unit area (eqn. 1) by the area of the simulation (36 Mm^2). Since our simulation domain is large enough to include a mesogranule, the pressure fluctuations are nearly uncorrelated on larger scales and the average pressure fluctuation squared decreases as the inverse of the area. There is a small correlation left from large mesogranules and supergranules which is not modeled in the simulation. The simulated solar excitation rates are in good agreement with the

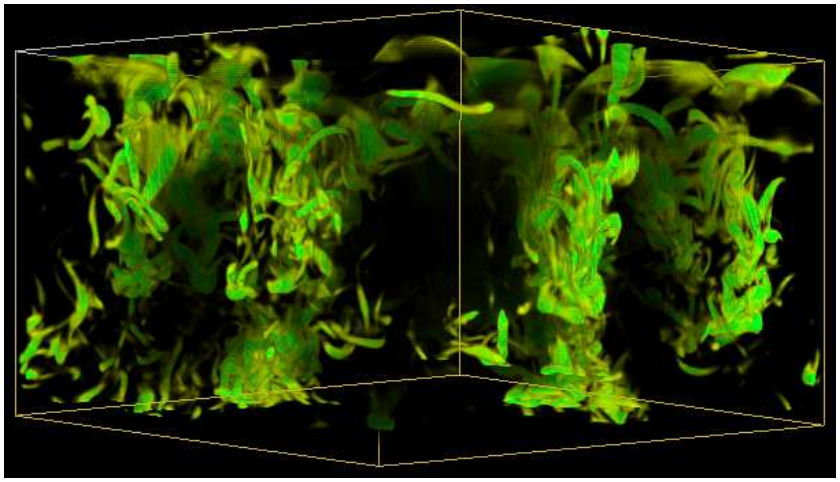

Figure 3. Vorticity image. Most of the vorticity is concentrated in the turbulent downdrafts as shown by the twisted vortex tubes.

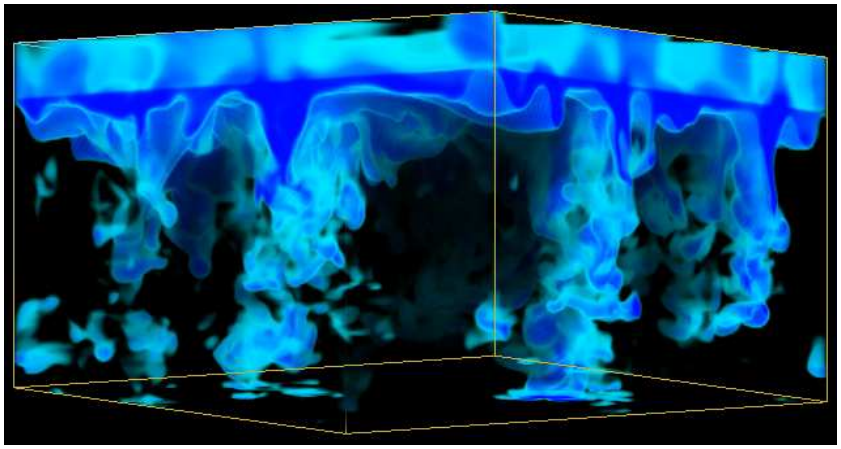

Figure 4. Entropy image. The downdrafts have large entropy fluctuations (blue & green) while the upflows have nearly uniform entropy.

solar observations from SOHO (Fig. 6). The excitation decreases at low frequencies because of the mode properties: the mode mass (or mode energy, E, in the denominator of eqn. 1) increases toward lower frequencies (Fig. 6 and mode compression ($\partial\xi/\partial z$) in the numerator of eqn. 1) decreases toward lower frequencies (Fig. 7). The excitation decreases at high frequencies because of the convection properties: convection is a low frequency phenomenon, so the turbulent pressure and non-adiabatic gas pressure (entropy) fluctuations (P^* in eqn. 1) it produces decrease at high frequencies (Fig. 7) (Stein & Nordlund 2001).

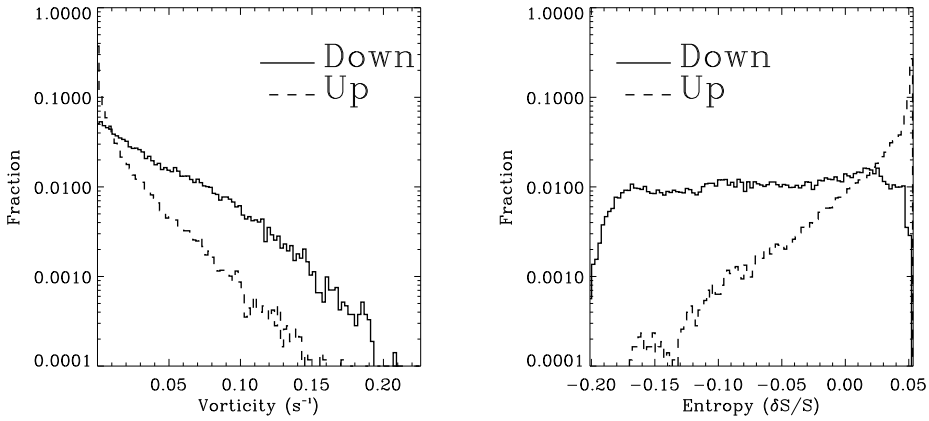

Figure 5. Vorticity (left) and entropy (right) probability distribution function separately for upflows and downflows near the surface.

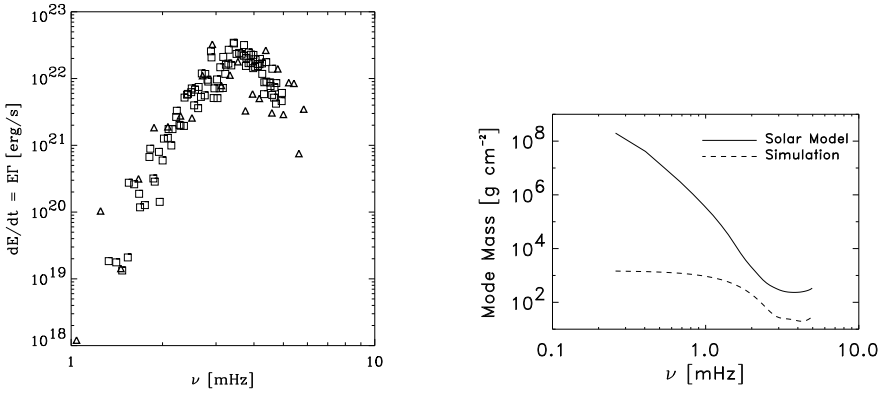

Figure 6. Comparison of observed and calculated p-mode excitation rates for the entire Sun left). Squares are from SOHO golf observations for $\ell = 0-3$ (Roca Cortes et al. 1999) and triangles are the simulation calculations. Mode mass for Solar and simulation modes (right). Mode mass increases at lower frequencies because the eigenfunctions extend deeper. The mass of the simulation modes becomes constant because the computational domain is limited in depth.

P-mode excitation occurs close to the top of the convection zone, in the superadiabatic layer, where the turbulent velocities and the entropy fluctuations are largest (Fig. 8). At low frequencies the overall driving is weaker, but it is spread fairly uniformily over a large depth. The peak driving is confined to a about 0.5 Mm of the surface. At high frequencies the driving becomes more and more concentrated close to the surface.

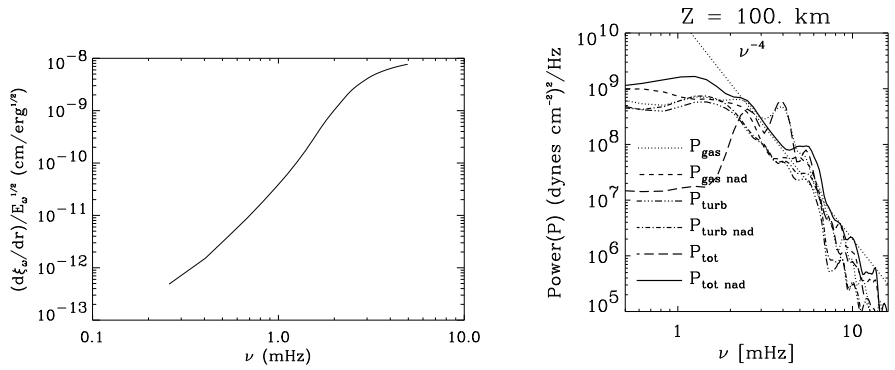

Figure 7. Mode compression (left) and pressure spectrum (right). The mode compression decreases toward low frequencies as the eigenfunctions vary more slowly, $k \approx \omega^2/g$. Both the turbulent and non-adiabatic gas pressure fluctuations decrease at high frequencies because the convective power decreases at high frequencies.

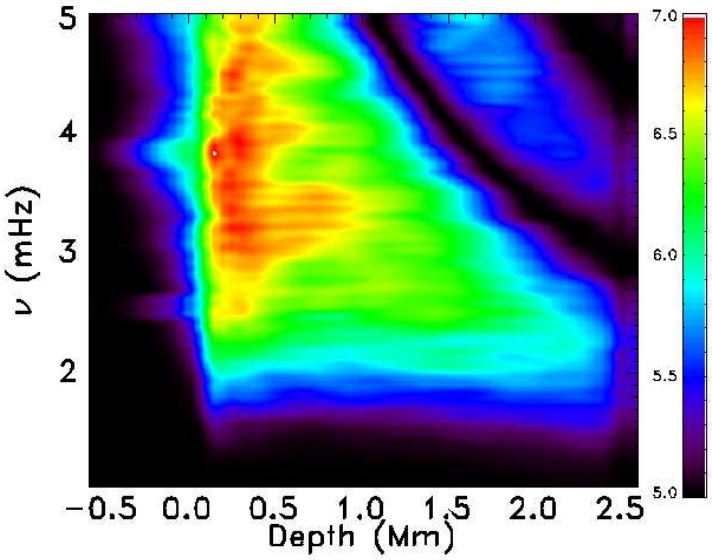

Figure 8. Logarithm (base 10) of the work integrand, $\omega^2 \left|\delta P_\omega^* \frac{\partial \xi_\omega}{\partial z}\right|^2 / 8\Delta\nu E_\omega$, (eqn 1) (in units of ergs/cm^2/s) as a function of depth and freqency. The driving is concentrated close to the surface.

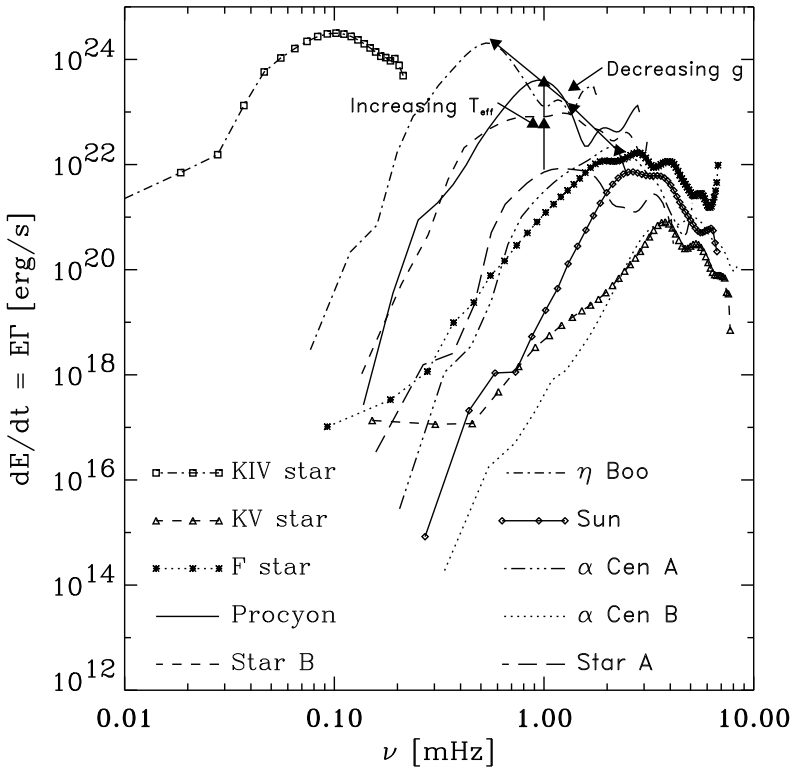

Figure 9. Excitation spectra of stars with different surface gravity and effective temperature. Maximum driving increases and occurs at lower frequencies for lower gravity. Drivinge increases with increasing effective temperature (until convection ceases for early F stars).

6. Stellar Excitation Rates

Simulations of convection in other stars have been used to calculate their p-mode excitation rates. As the surface gravity of the stars decreases the maximum excitation rate increases and shifts to lower frequency (Fig. 9). As the effective temperature of the stars increases (until surface convection ceases in the F stars) the excitation rate increases while the frequency of maximum driving remains unchanged (Fig. 9). Maximum driving shifts to lower frequency with decreasing surface gravity because the buoyancy frequency and the acoustic cutoff frequency both decrease. The excitation rate increases with increasing effective temperature because a larger convective flux requires larger velocity and temperature fluctuations to transport more energy.

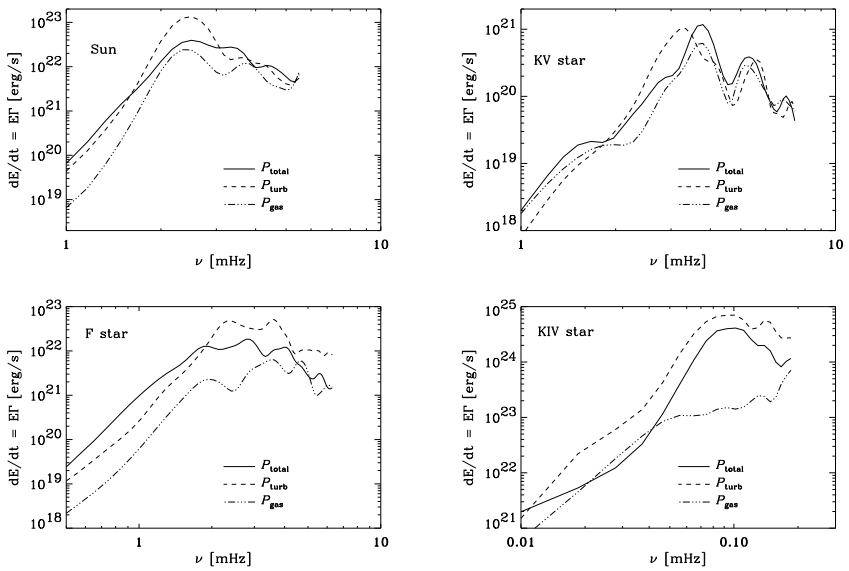

Figure 10. Total excitation and individual contributions from turbulent and non-adiabatic gas pressure fluctuations for the Sun, F, K V and K IV stars. For most main sequence stars the contributions from the two individual source are nearly comparable, but for the hottest F star and the subgiant K IV star the turbulent pressure driving dominates.

Turbulent pressure and non-adiabatic gas pressure contribute approximately equally (the turbulent pressure is slightly larger) to the mode excitation of most of the main sequence stars. For the hottest F star and for the subgiant K IV star the mode driving by turbulent pressure is significantly larger than the driving by the non-adiabatic gas pressure (Fig. 10). Note that the total excitation is not equal to the sum of the individual turbulent and non-adiabatic gas pressure contributions. Sometimes there is destructive interference between them. The individual contributions of turbulent pressure and non-adiabatic gas pressure fluctuations to the frequency integrated excitation for the entire stars as a function of effective temperature and surface gravity is shown in Fig. (11).

The frequency integrated total excitation rate for the entire star is shown as a function of effective temperature and surface gravity in Fig. (12). The increase of driving with increasing effective temperature and decreasing surface gravity is clearly revealed.

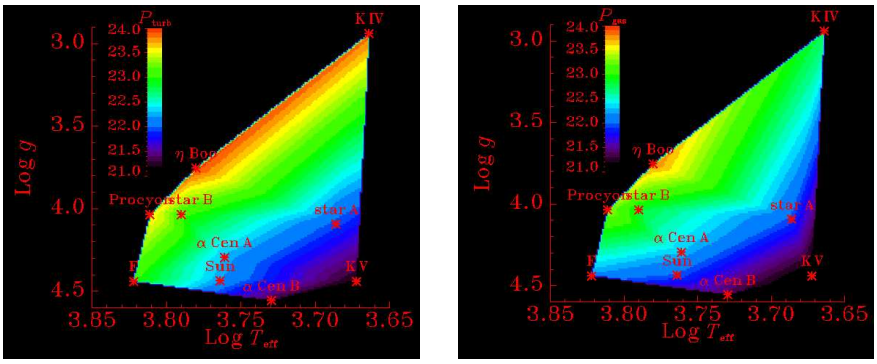

Figure 11. Individual contributions of turbulent (left) and non-adiabatic gas pressure (right) fluctuations to the frequency integrated excitation for the entire star.

7. Summary

P-modes are excited by the work of turbulent pressure (Reynolds stresses) and non-adiabatic gas pressure (entropy) flucuations. The excitation decreases at low frequencies because of mode propertiers: the mode mass increases and the mode compression decreases toward lower frequencies. The excitation decreases toward high frequencies because of convection properties: convection has little high frequency motions and so produces little high frequency turbulent or non-adiabatic gas pressure fluctuations. The results of calculating the excitation of a few main sequence and one cool sub-giant star show that mode excitation increases with increasing effective temperature and decreasing surface gravity.

Acknowledgements

This work was supported in part by NASA grants NAG 5 9563 and NAG 5 12450 and NSF grant 0205500. Their support is greatly appreciated.

References

Balmforth, N. J.: 1992, Monthly Notices Royal Astron. Soc., **255**, 639.
Bedding, T. R. and Kjeldsen, H.: 2003, Publ. Astron. Soc. Australia, **20**, 203.
Bohm-Vitense, E.: 1958, Zeits. f. Astrophys. **46**, 108.
Canuto, V. M. and Mazzitelli, I.: 1991, Astrophys. J., **370**, 295.
Deubner, F.-L.: 1975, Astron. Astrophys., **44**, 371, 1975.
Goldreich, P. and Keely, D. A.: 1977, Astrophys. J., **212**, 243.

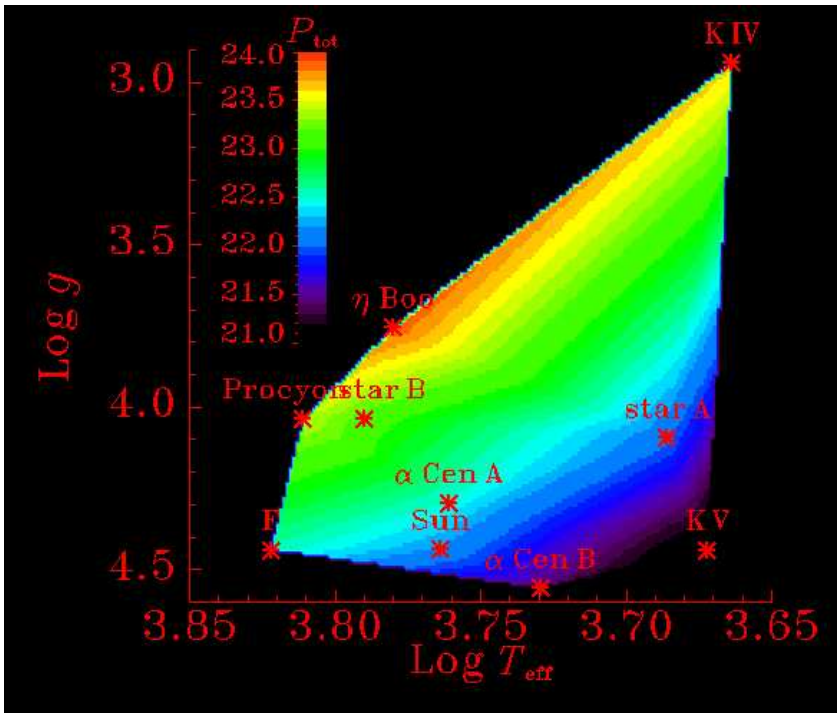

Figure 12. Frequency integrated total excitation rate for the entire star, increases with increasing effective temperature and decreasing surface gravity.

Goldreich, P., Murray, N. and Kumar, P.: 1994, Astrophys. J., **424**, 466.

Hyman, J.: 1979, in R. Vichnevetsky and R. S. Stepleman eds. *Advances in Computer Methods for Partial Differential Equations III*, p. 313.

Ludwig, H.-G. and Nordlund, Å.: 2000, in L. S. Cheng, H. F. Chau, K. L. Chan, and K. C. Leung eds. *Proceedings of the Pacific Rim Conference, Hong Kong 1999*, Kluwer Academic Publishers, The Netherlands.

Nordlund, Å.: 1982, Astron. Astrophys., **107**, 1.

Nordlund, Å. and Stein, R. F.: 1991, in *Stellar Atmospheres: Beyond Classical Models*, D. Reidel, Dordrecht, p 263.

Nordlund, Å. and Stein, R. F.: 2001, Astrophys. J., **546**, 576.

Roca Cortes, T., Montanes, P., Palle, P. L., Perez Hernandez, F., Jimenez, A., Regula, C. and the GOLF Team: 1999, in A. Gimenez, E. Guinan, B. Montesinos eds., *Theory and Tests of Convective Energy Transport*, ASP Conf. Ser. **173**, 305.

Samadi, R. and Goupil, M.-J.: 2001, Astron. Astrophys., **370**, 136.

Stein, R. F. and Nordlund, Å.: 1998, Astrophys. J., **499**, 914.

Stein, R. F. and Nordlund, Å.: 2000, Sol. Phys. **192**, 91.

Stein, R. F. and Nordlund, Å.: 2001, Astrophys. J., **546**, 585.

Stein, R. F. and Nordlund, Å.: 2003, in I. Hubeny, D. Mihalas and K. Werner, eds. *Stellar Atmosphere Modeling*, ASP conf. proc., **288**, 519.

Trampedach, R., Steinr, R. F., Christensen-Dalsgaard, J. and Nordlund, Å.: 1998, in A. Gimeénez, E. F. Guinan, B. Montesinos eds., *theory and Tests of Convection is Stellar Structure*, ASP conf. series, 233-236.